Journal of Materials Chemistry C

ROYAL SOCIETY OF CHEMISTRY

PAPER

View Article Online
View Journal | View Issue

Cite this: J. Mater. Chem. C, 2022, 10, 11040

A Cr^{3+} luminescence based ratiometric optical laser power meter†

L. Marciniak, *[a] M. Szalkowski,[ab] A. Bednarkiewicz [a] and K. Elzbieciak-Piecka[a]

Received 5th June 2022,
Accepted 5th July 2022

DOI: 10.1039/d2tc02348b

rsc.li/materials-c

Chromium doped luminescent phosphors display numerous spectral features that can be useful for designing modern multi-functional materials. Here we study $GdAl_3(BO_3)_4$ nanoparticles doped with Cr^{3+} ions, which enable combining efficient light-to-heat conversion and efficient luminescent properties in homogenously doped materials avoiding complicated syntheses of hetero-structural or hybrid-designed materials. In particular, while the intentionally increased content of Cr^{3+} ions leads to increased self-heating in a relatively broad photoexcitation spectrum, the concurrently occurring bright luminescence intensity ratio between the $^4T_{2(g)}$ level and the $^2E_{(g)}$ level responds to local temperature variation. Such behavior inspired us to evaluate the possibility of ratiometrically measuring the delivered laser pump power. The presented strategy enables the development of luminescent sensors operating in a wide range of power densities. It has been proposed and explained how the performance of the sensor, including sensitivity and usable excitation density range of optical density meter, can be modified by the knowledgeable optimization of the Cr^{3+} dopant ion concentration. We believe that this work may be the beginning of a new research direction that will allow the development of highly sensitive remote optical density meters.

Introduction

Nonradiative relaxation is typically considered as detrimental for luminescence and many efforts have been undertaken to prevent it.[1–5] In the case of materials doped with lanthanide ions, low phonon energy matrices and low dopant concentrations were proposed, mostly to eliminate multiphonon relaxation processes.[6,7] On the other hand, for transition metal ions, the preservation of a small shift between the parabolas of the excited and ground levels and a small electron-phonon coupling were found to reduce the probability of nonradiative processes.[8–10] Satisfying these requirements enables maintaining intense luminescence even at increased temperatures. Nevertheless, judicious exploitation of nonradiative processes and a wise combination of these features with other inherent properties of the luminescent nanoparticles allow developing luminescence-based multifunctional materials.[11–13] For example, strong susceptibility of nonradiative processes rates on parameters such as temperature, pressure and pH facilitates the development of luminescent sensors of those physical and chemical quantities. Simultaneously, purposeful enhancement of these processes may be additionally suitable for photothermal therapy of cancer.[14–16] The intentional management of probability of nonradiative processes can be achieved by adopting appropriate nanoparticle compositional architecture[17] or by exploiting appropriate optical excitation wavelengths.[18] The capability of accommodating efficient light to heat conversion with simultaneous susceptibility of ratiometric luminescence spectra to temperature within single phosphor enables designing multifunctional materials. Such phosphors may be applied to measure the excitation power.

Here we study $GdAl_3(BO_3)_4$ nanoparticles doped with Cr^{3+} ions as a model material. The choice of the host material and luminescent active ions was motivated by their unique properties (Fig. 1). Luminescence of Cr^{3+} ions occurs, depending on the strength of the interacting crystal field, from $^2E_{(g)}$ and/or $^4T_{2(g)}$.[19–24] In the case of a strong crystal field, the emission spectrum is dominated by the spectrally narrow band associated with the $^2E_{(g)} \rightarrow {}^4A_{2(g)}$ electronic transition, whereas in the case of a weak crystal field, the emission spectrum of Cr^{3+} ions consists of the broad $^4T_{2(g)} \rightarrow {}^4A_{2(g)}$ band. Both energy levels are thermally coupled, *i.e.*, for strong and intermediate crystal field host materials, an increase in temperature results in an increase in the population of the $^4T_{2(g)}$ level with respect to $^2E_{(g)}$. Therefore in the case of intermediate crystal field materials for which both emission bands are observed in the spectrum, an increase in the probability of nonradiative processes involved in

[a] Institute of Low Temperature and Structure Research, Polish Academy of Sciences, Okólna 2, 50-422 Wroclaw, Poland. E-mail: l.marciniak@intibs.pl
[b] Institute of Physics, Faculty of Physics, Astronomy and Informatics, Nicolaus Copernicus University, Grudziądzka 5, 87-100 Toruń, Poland

† Electronic supplementary information (ESI) available. See DOI: https://doi.org/10.1039/d2tc02348b

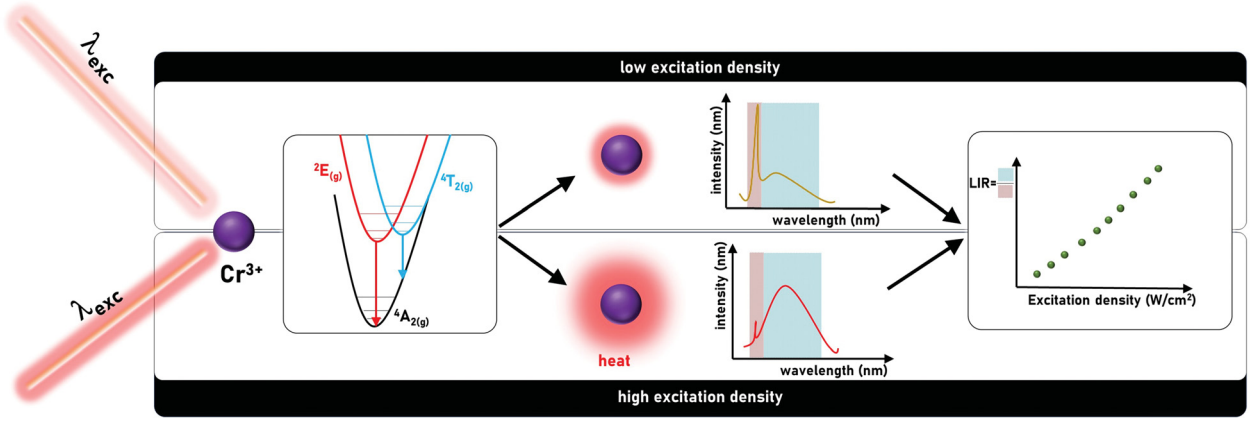

Fig. 1 Schematic representation of the principle of operation of Cr^{3+} based ratiometric laser power meter: the luminescence spectra of Cr^{3+} ions in $GdAl_3(BO_3)_4$ consist of two emission bands associated with the radiative transitions from both $^2E_{(g)}$ and $^4T_{2(g)}$ states. Upon low excitation density (top), low heat is generated, hence the $^2E_{(g)} \rightarrow {}^4A_{2(g)}$ emission band dominates in the spectrum, whereas upon high excitation density (bottom), high heat generated in the system leads to the thermalization of the $^4T_{2(g)}$ state and thus a relative increase of the $^4T_{2(g)} \rightarrow {}^4A_{2(g)}$ band intensity with respect to the $^2E_{(g)} \rightarrow {}^4A_{2(g)}$ is observed. Therefore, the LIR of these two bands can be exploited as a measure of laser beam power.

the conversion of light to heat will contribute to an increase in the emission intensity of $^4T_{2(g)} \rightarrow {}^4A_{2(g)}$ with respect to the $^2E_{(g)} \rightarrow {}^4A_{2(g)}$. The increase in the temperature of the phosphor depends on the efficiency of the light to heat conversion processes and the excitation power density. Hence, the ratio of the emission intensity associated with the $^4T_{2(g)} \rightarrow {}^4A_{2(g)}$ and $^2E_{(g)} \rightarrow {}^4A_{2(g)}$ bands can be exploited as a luminescent optical excitation density indicator. To enhance the sensitivity of this optical power meter, a high concentration of Cr^{3+} ions was used to facilitate energy migration to the killer centers. The $GdAl_3(BO_3)_4$ belongs to the family of the $RX_3(BO_3)_4$,[25,26] which is very frequently used as a host material for Cr^{3+} based phosphors. The modification of the host material composition significantly affects the spectroscopic properties of the phosphor. Low temperature emission spectra of $YAl_3(BO_3)_4$:Cr^{3+} are dominated by the $^2E \rightarrow {}^4A_2$ emission band whereas the $^4T_2 \rightarrow {}^4A_2$ band cannot be observed.[27–29] Although the emission intensity of $^4T_2 \rightarrow {}^4A_2$ increases at room temperature, the spectrum is still dominated by the $^2E \rightarrow {}^4A_2$ band.[30] When Y^{3+} ions are replaced by Gd^{3+} the $^4T_2 \rightarrow {}^4A_2$ emission intensity starts to dominate over the $^2E \rightarrow {}^4A_2$ band. More spectacular changes in the shape of the emission band, however, are found when the Al^{3+} ions are substituted by Sc^{3+}. This directly affects the shape of the octahedra surrounding the Cr^{3+} ions and thus only the $^4T_2 \rightarrow {}^4A_2$ band can be observed for $YSc_3(BO_3)_4$:Cr^{3+} and $GdSc_3(BO_3)_4$:Cr^{3+}.[30] Brik *et al.* revealed that when Cr^{3+} occupies the distorted octahedral site of Sc^{3+} ions in $(Ce,Gd)Sc_3(BO_3)_4$:Cr^{3+} the intense broad band of the $^4T_2 \rightarrow {}^4A_2$ electronic transition with the maxima at 910 nm can be achieved.[31] Replacement of Gd^{3+} by larger La^{3+} results in the change of the emission band maxima to 963 nm in $LaSc_3(BO_3)_4$.[32–34] Wu *et al.* proposed a strategy that when the Y^{3+} ions are introduced into the system to occupy partially La^{3+} and Sc^{3+} sites, the significant blue shift of the emission band to the 850 nm in $Y_{0.57}La_{0.72}Sc_{2.71}(BO_3)_4$:Cr can be observed.[35]

The $GdAl_3(BO_3)_4$ host material is characterized by two important advantages especially beneficial for the purpose of this study. First of all, it consists of an Al^{3+} octahedral site which could be occupied by the Cr^{3+} ions and even a high dopant concentration does not affect the crystal field strength. Second, it is characterized by high phonon energy which further increases the probability of light-to-heat conversion required for the developed application.[36–38] Besides, $GdAl_3(BO_3)_4$ is highly mechanically and thermally stable which enables developing a laser beam power meter operating even in the high excitation power density range without any degradation or decomposition of the material. The spectrally broad absorption bands of Cr^{3+} ions in the visible range associated with the $^4A_{2(g)} \rightarrow {}^4T_{1(g)}$ and $^4A_{2(g)} \rightarrow {}^4T_{2(g)}$ electronic transitions allow for extending the useful spectral range for which the luminescence response of the developed power meter will be recorded. Understanding the photophysics and materials sciences, let us propose a new method to measure the laser beam power as a simple proof-of-concept demonstration of multi-functional luminescent nanoparticles.

Experimental

Synthesis

Gadolinium(III) oxide (Gd_2O_3 REacton 99.999% purity, Alfa Aesar), aluminum(III) nitrate hydrate ($Al(NO_3)_3 \cdot 9H_2O$ Puratronic 99.999% purity, Alfa Aesar), chromium(III) nitrate hydrate ($Cr(NO_3)_3 \cdot 9H_2O$ 99.99% purity, Alfa Aesar), boric acid (H_3BO_3 99.97% purity, Aldrich Chemistry), D-sorbitol ($C_6H_{14}O_6$ > 98.0% purity POL-AURA), citric acid ($C_6H_8O_7$ 99% purity, Sigma-Aldrich), and *n*-hexane (Avantor) were used as the starting materials for synthesis without further purification.

The $GdAl_3(BO_3)_4$ borates doped with (1; 5; 10)% Cr^{3+} were synthesized according to the modified polymer precursor method, described in detail in previous work.[39,40] In general, this method consist of the complexation of metal cations by given carboxylic acid (*e.g.* citric acid) and further polymerization

reaction which occurs between the used carboxylic acid and polyhydroxyl alcohol (*e.g.* D-sorbitol) resulting in the formation of a polymeric resin. In order to compensate for the loss of boric acid due to its evaporation during the synthesis and annealing process, an appropriate excess of both Al^{3+} and B^{3+} ions. The ratios were estimated on the basis of the percentage of the additional $GdBO_3$ phase received from X-ray powder diffraction patterns. First, gadolinium nitrate was obtained through the dissolution of gadolinium oxide in slightly diluted hot ultrapure nitric acid followed by a triple recrystallization process. Then, appropriate amounts of gadolinium, aluminum and chromium nitrates were dissolved in deionized water and an aqueous solution of citric acid was added in order to form citrate complexes of metal ions. Citric acid was added in the ratio of 3 : 1 with respect to the number of moles applied to the metal and boron ions and in the ratio of 3 : 2 with respect to D-sorbitol. Subsequently, an earlier prepared solution of D-sorbitol and boric acid was added and then the complete solution was stirred for 3 h at about 100 °C. Then, the solutions were heated for a few days at 90 °C to obtain crumbly resins. Afterward, the resins were pre-calcined under the following conditions: 400 °C/16 h and 700 °C/16 h with a heating rate of 5 °C min^{-1} under an air atmosphere, with grinding in *n*-hexane between successive annealing processes. Such prepared powders were annealed at 1100 °C for 5 h.

Characterization

The X-ray powder diffraction (XRPD) patterns were measured with the use of a PANalitycal X'Pert diffractometer, equipped with an Anton Paar TCU 1000 N temperature control unit, using Ni-filtered Cu-K_α radiation (V = 40 kV, I = 30 mA). Transmission electron microscopy images were taken on a Philips CM-20 SuperTwin microscope using an accelerating voltage of 160 kV and a 0.25 nm spatial resolution. Excitation spectra and luminescence decay profiles were recorded using an FLS 1000 fluorescence spectrometer from Edinburgh Instruments equipped with a R928P side window multiplier tube from Hamamatsu as a detector as well as a 450 W halogen lamp and a μFlash lamp (40 Hz repetition, 20 ms time width of the excitation pulse) as the excitation sources. The temperature increase curves and thermovision images were collected using a T540 camera from FLIR.

The excitation power dependent emission spectra were collected using a home-built optical setup, illustrated schematically in Fig. S1 (ESI†). The excitation beam (445 nm) provided by the laser diode was collimated and then passed through the neutral filter with variable optical density (NDM4/M, Thorlabs), used to adjust the power density of the excitation beam. Next, this beam was split into two fractions – one part was transmitted by the beam splitter and was focused with an objective lens (Genetic Pro, Plan 20×, NA = 0.40, Delta Optical) on the sample enclosed in a quartz cuvette, while the other part of the light was reflected (R = 3%) by the beam splitter and directed to the power meter head (S121C, Thorlabs) connected with the computer to monitor the power of the beam. This reference power is proportional to the power of the light transmitted by the beam splitter, therefore the power of the light illuminating sample was possible to reconstruct. The light emitted by the sample was then collected by the lens and, and after passing through the longpass filter (FEL0600, Thorlabs), it was focused on the entrance slit (10 μm) of the spectrograph (Shamrock 500i, Andor) equipped with a CCD camera (Newton 920, BEX2-DD, Andor) to record the emission spectra. All of the recorded spectra were collected with an acquisition time of 50 ms.

Results and discussion

The $GdAl_3(BO_3)_4$ crystallizes in a trigonal crystal system with a R_{32} (no. 155) space group isostructural to $CaMg_3(CO_3)_4$.[36–38,41] It consists of octahedrally coordinated Al^{3+} sites and octahedrally coordinated Gd^{3+}, $(BO_3)^{3-}$ groups are arranged in sheets of planar triangles. Due to the similarities in the ionic charge and the ionic radii the Al^{3+} sites of C_2 point symmetry are preferentially occupied by the Cr^{3+} ions. Due to the relatively large Al^{3+}–O^{2-} bond length (1.902 A) and the intermetallic Al^{3+}–Al^{3+} distance even the high concentration of Cr^{3+} (up to 10% molar in respect to the Al^{3+} ions) does not affect the average Cr^{3+}–O^{2-} distance and thus the crystal field strength. The XRD patterns measured for $GdAl_3(BO_3)_4$ powders indicate that independently of Cr^{3+} concentration, pure-phased $GdAl_3(BO_3)_4$ structures were obtained (Fig. 2b). The representative TEM images of the $GdAl_3(BO_3)_4$:Cr^{3+} powders reveal that the synthesized $GdAl_3(BO_3)_4$ consists of submicrometric well-crystallized particles of an average size of around 400 nm (Fig. 2c–e). Additionally, no visible influence of the dopant concentration on the morphology of synthesized powders was observed

The luminescence spectra of materials doped with Cr^{3+} ions result from the d–d electronic transitions. In the case of the transition metal ions of $3d^3$ electronic configuration observed for Cr^{3+} ions, depending on the crystal field strength of the host material the spectrum is dominated either by narrow band $^2E_{(g)} \rightarrow {}^4A_{2g}$ emission (strong crystal field) or broad emission band $^4T_{2(g)} \rightarrow {}^4A_{2(g)}$ for the weak crystal field. However, in order to develop a ratiometric optical excitation density sensor based on the emission intensity ratio from the $^2E_{(g)}$ level to that from the $^4T_{2(g)}$ level, one should use materials with an intermediate crystal field for which both bands are observed in the spectrum simultaneously (Fig. 3a). Therefore, $GdAl_3(BO_3)_4$ was used as a host material in this study. Representative emission spectra recorded for 200 mW cm^{-2} of λ_{exc} = 445 nm optical excitation at room temperature shown in Fig. 3b reveal a strong dependence of the emission spectra on the Cr^{3+} ion concentration. As the Cr^{3+} content increases, the intensity of the broad $^4T_{2(g)} \rightarrow {}^4A_{2(g)}$ band increases relative to the $^2E_{(g)} \rightarrow {}^4A_{2(g)}$ one. Although such a change may suggest a modification in the crystal field strength with increasing dopant ion concentrations,[42] a careful analysis of the excitation spectra clearly indicates that the positions of the $^4A_{2(g)} \rightarrow {}^4T_{2(g)}$ and $^4A_{2(g)} \rightarrow {}^4T_{1(g)}$ absorption bands of Cr^{3+} ions are independent of the dopant ion concentration. The determined strength of the crystal field (based on eqn (S1)–(S3), ESI†) confirms this observation and $Dq/B \sim 2.48$ is obtained for all analyzed dopant concentrations (Fig. 3c).

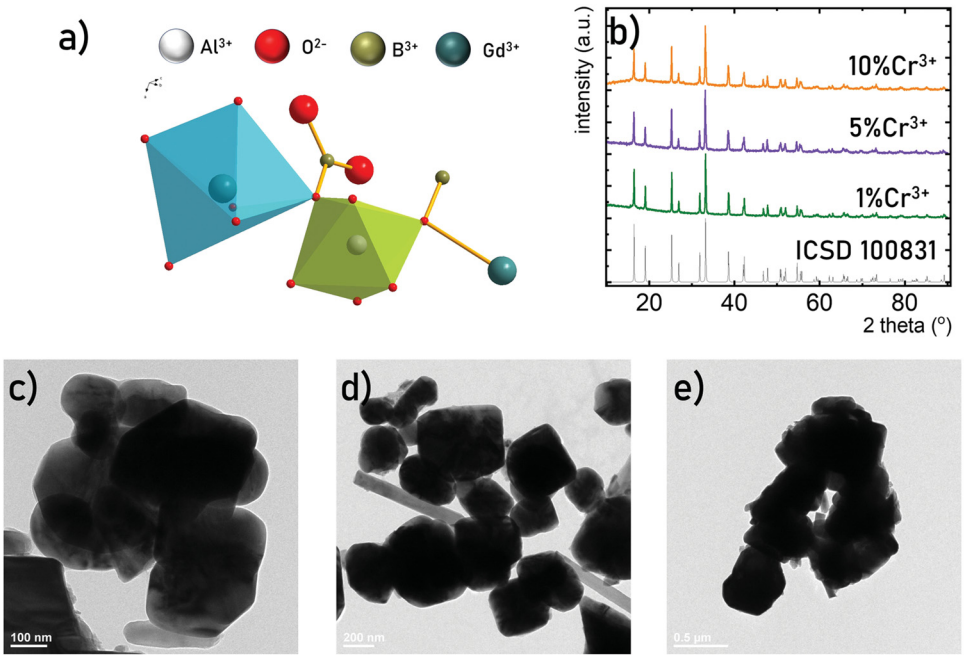

Fig. 2 Visualization of the octahedral $(AlO_6)^{9-}$ and octahedral $(GdO_6)^{9-}$ sites in $GdAl_3(BO_3)_4$ (a) and the XRD patterns of $GdAl_3(BO_3)_4$:Cr^{3+} doped with different concentrations of Cr^{3+} ions (b) and representative TEM images of the $GdAl_3(BO_3)_4$:1%Cr^{3+} (c) and $GdAl_3(BO_3)_4$:10%Cr^{3+} (d and e).

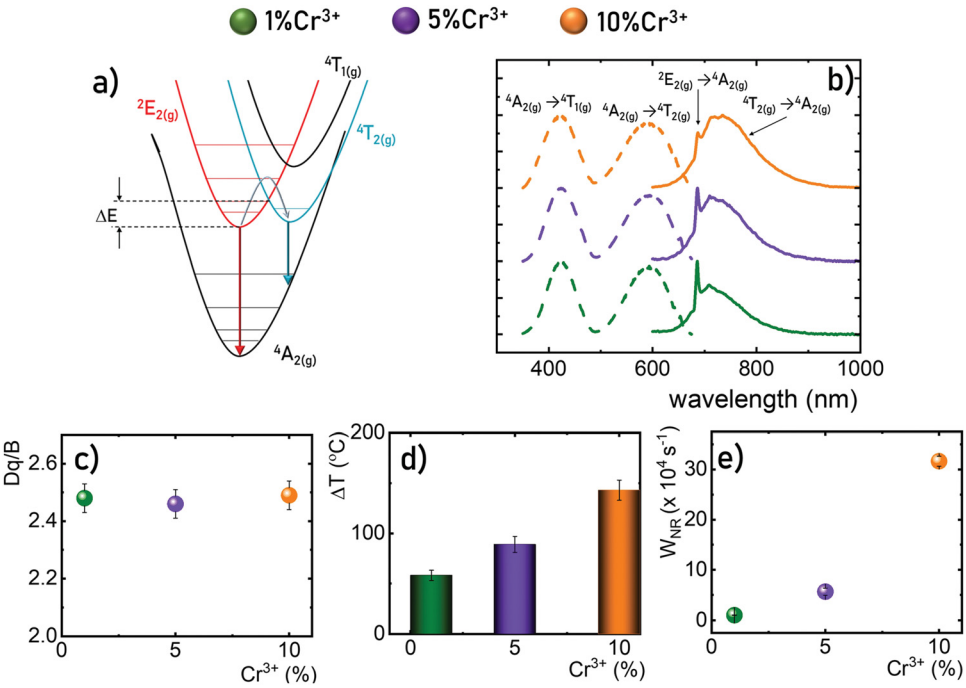

Fig. 3 Simplified configurational coordination diagram of the Cr^{3+} energy levels in an intermediate crystal field strength (a), room temperature emission (λ_{exc} = 445 nm, solid line) and excitation (λ_{em} = 690 nm, dashed line) spectra of $GdAl_3(BO_3)_4$:Cr^{3+} (b); the influence of the Cr^{3+} concentration on the *Dq*/*B* (c); the temperature of the powder upon 2 W cm^{-2} of λ_{exc} = 445 nm optical excitation determined using a thermovision camera (d) and probability of nonradiative processes (e).

Thus, the observed change in the shape of the emission spectrum can be explained by more efficient thermalization of the $^4T_{2(g)}$ level relative to the $^2E_{(g)}$ level for high dopant concentrations. The enhanced efficiency of the light to heat conversion process in materials with high Cr^{3+} ion concentrations is related to two factors. The first of them is a more efficient absorption of the excitation radiation associated with an increase in the absorption cross-section observed for heavily

doped particles. The second effect is related to a more efficient diffusion of energy across the excited levels of Cr^{3+} ions to killing centers. When such a center is reached the nonradiative recombination of the electron takes place. The probability of this process increases with the concentration of Cr^{3+} ions. The interaction of these two effects promotes efficient optical heating of the phosphor. To confirm this hypothesis, the temperature of the $GdAl_3(BO_3)_4$:Cr^{3+} powders upon a constant optical excitation density of 2 W cm^{-2} was observed using a thermovision camera (Fig. 3d). The results obtained after 2 minutes of continuous optical excitation clearly indicate that while for $GdAl_3(BO_3)_4$:1%Cr^{3+} the recorded temperature was 58 °C, 143 °C was recorded for $GdAl_3(BO_3)_4$:10%Cr^{3+}. The efficient depopulation of the $^2E_{(g)}$ level by thermalization with increasing Cr^{3+} ion concentrations is also reflected in the kinetics of the luminescence. The determined probability of nonradiative processes (from eqn (S4), ESI†) clearly increases with increasing Cr^{3+} ion concentrations. These results confirm that the material efficiently converts light to heat and a clear indicator of this may be the shape of the $GdAl_3(BO_3)_4$:Cr^{3+} emission spectrum.

To experimentally verify the hypothesis that an emission intensity ratio of Cr^{3+} ions can be exploited to develop a ratiometric optical excitation power density sensor, the emission spectra of $GdAl_3(BO_3)_4$:Cr^{3+} were recorded as a function of 445 nm optical excitation power density from 1.2 to 4300 W cm^{-2}. The representative spectra of the $GdAl_3(BO_3)_4$:1%Cr^{3+} clearly show that besides a significant increase in emission intensity, the shape of the emission spectrum also changes with photoexcitation density (Fig. 4a). With increasing laser beam power density the intensity of the $^4T_{2(g)} \rightarrow {}^4A_{2(g)}$ band significantly increases with respect to the $^2E_{(g)} \rightarrow {}^4A_{2(g)}$ band and for 4300 W cm^{-2} the intensity of both bands is comparable. Analogous changes are also observed for the samples with the other concentrations (Fig. S2 and S3, ESI†). However, the dynamics of these changes for the power density regime below 1000 W cm^{-2} increase with the increasing dopant ion concentration. In order to quantitatively describe the observed changes in the shape of the emission spectrum, the emission intensity ratio (LIR) is defined as follows:

$$\mathrm{LIR} = \frac{\int_{735\,\mathrm{nm}}^{750\,\mathrm{nm}} {}^4T_{2(g)} \rightarrow {}^4A_{2(g)} d\lambda}{\int_{678\,\mathrm{nm}}^{693\,\mathrm{nm}} {}^2E_{2(g)} \rightarrow {}^4A_{2(g)} d\lambda} \quad (1)$$

As can be observed for samples with low Cr^{3+} ion concentrations, the LIR is a linear function of the optical excitation power density and increases monotonically from 2.23 to 2.94 in the 1.3 to 4300 W cm^{-2} excitation density range (Fig. 4b). However, the growing number of dopant ions clearly affects the LIR. For 5%Cr^{3+} the LIR in the same range of excitation power density increases from 2.68 to 4.52, whereas for 10% Cr^{3+}, it increased from 3.17 to 4.93. Significantly, for high dopant ion concentrations the most rapid increase in the LIR is observed below 2700 W cm^{-2} and 1800 W cm^{-2} for 5%Cr^{3+} and 10%Cr^{3+}, respectively. Above these power density values, the LIR begins to saturate and a further increase of the excitation density does not lead to a meaningful change in the LIR. A qualitative description of these changes can be achieved by analyzing the absolute sensitivity of the luminescent power meter defined as follows:

$$S_A = \frac{\Delta \mathrm{LIR}}{\Delta P} \quad (2)$$

where ΔLIR represents the change in the LIR corresponding to a ΔP change in power density. In the case of 1%Cr^{3+}, S_A takes an almost constant value over the entire range of the analyzed power density equal to S_A = 0.18 W^{-1}. On the other hand, for 10%Cr^{3+}, S_A reaches very high values for low excitation power densities S_A = 2.68 W^{-1} for 2 W cm^{-2} and increasing the power density causes a monotonic decrease in S_A. It should be noted here that for power densities above 1700 W cm^{-2}, S_A values fall below those reported for 1%Cr^{3+}. This result confirms that high dopant ion

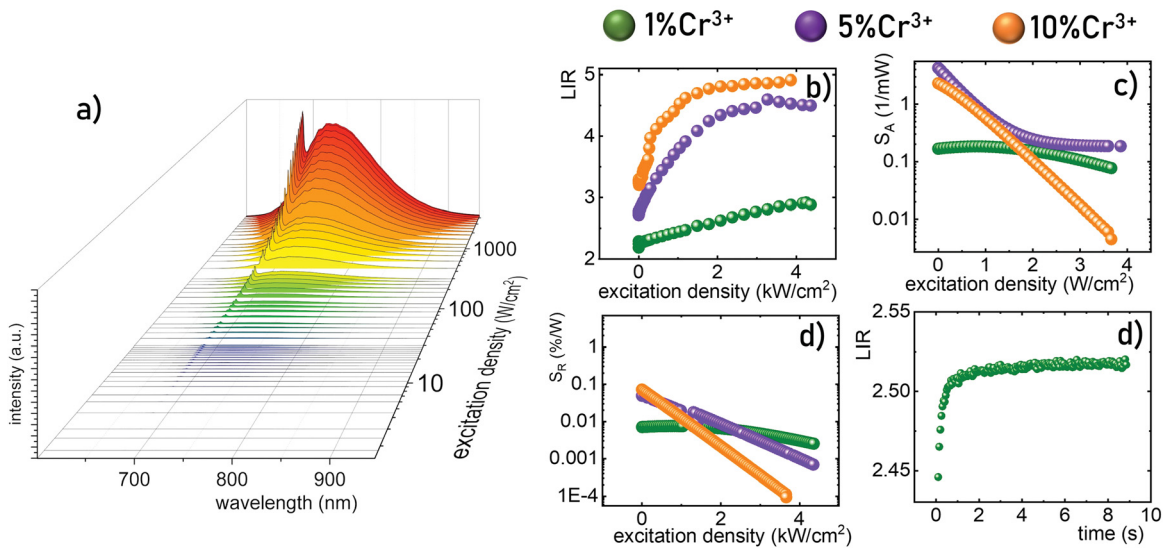

Fig. 4 Emission spectra of $GdAl_3(BO_3)_4$:1%Cr^{3+} recorded as a function of excitation density of λ_{exc} = 445 nm (a); the dependence of luminescence intensity ratio (LIR) of 2E → 4A2 to 4T2 → 4A2 bands on excitation density dependence (b).

concentrations are preferable for the development of low excitation density luminescence based sensors. However, very interesting results were observed for the 5%Cr^{3+} sample. In this case, for 1.2 W cm^{-2} even a higher value of S_A = 5.11 W^{-1} was observed exceeding that observed for 10%Cr^{3+}. However, even for the higher power density regime, the observed S_A is slightly higher than that for the 1%Cr^{3+} counterpart. Above 2.23 W cm^{-2}, the S_A, in this case, saturates at about 0.21 W^{-1}. Since the LIR is a dimensionless parameter, comparing the performance of different luminescence-based power meters is difficult to perform. For this purpose, a relative sensitivity parameter defined analogously to the parameter described for luminescence thermometry was introduced as follows:

$$S_R = \frac{1}{LIR}\frac{\Delta LIR}{\Delta P}\cdot 100\% \quad (3)$$

Similar to S_A, the lowest S_R values were recorded for 1%Cr^{3+} at about S_R = 0.07% W^{-1}. By increasing the concentration of Cr^{3+} ions, an increase in the maximum relative sensitivity was obtained for S_R = 0.05% W^{-1} and S_R = 0.07% W^{-1} for 5%Cr^{3+} and 10%Cr^{3+}, respectively. Analogously to S_A, the highest S_R values are observed for high dopant concentrations. However, it should be emphasized that increasing the concentration simultaneously narrows the useful power density range. In order to prove that the observed changes in the emission spectra of $GdAl_3(BO_3)_4$:Cr^{3+} are not related to the sample decomposition, and the LIR values for 11 cycles of high and low power density were examined. The obtained results confirmed the high reproducibility of the obtained results (Fig. S4, ESI†). For the design of a luminescence-based power meter, the response time of the sensor to a change in the excitation power density is important. For this purpose, the kinetics of LIR changes for a constant excitation power density of 2.3W cm^{-2} for $GdAl_3(BO_3)_4$:1%Cr^{3+} was investigated. It is clearly seen that after about 1s the LIR value assumes a constant value which indicates the sensitivity of the proposed meter to dynamic changes in the excitation power density. Changes in the shape of the emission spectrum under different excitation density conditions can be achieved not only for the λ_{exc} = 445 nm but for any wavelength matching the absorption bands of the Cr^{3+} ions (see for instance the emission spectra obtained for λ_{exc} = 532 nm – Fig. S5, ESI†).

Conclusions

In summary, this manuscript presents a strategy for the development of a remote optical excitation power density sensor. The described approach exploits the luminescence of Cr^{3+} ions in $GdAl_3(BO_3)_4$ – a host material and an intermediate crystal field material. In such a case both emission bands $^4T_{2(g)} \rightarrow {}^4A_{2(g)}$ and $^2E_{(g)} \rightarrow {}^4A_{2(g)}$ are observed in the luminescence spectrum and the thermal coupling occurring between the emitting levels results in the increase of the emission intensity from the $^4T_{2(g)}$ level with respect to the $^2E_{(g)}$ level at elevated temperatures. Therefore, an increase in the power density resulting in the heating of the phosphor in terms of light to heat conversion results in a change in the luminescence intensity ratio of these bands. After calibration, such LIR variations become a measure of laser beam optical power density. As expected, increasing the concentration of Cr^{3+} ions results in a higher absorption coefficient, higher probability of nonradiative processes and thus increasing the optically induced temperature of the phosphor. Hence, for low dopant concentrations (1%Cr^{3+}) a linear dependence of LIR on power density with relatively low absolute and relative sensitivity was observed. On the other hand, increasing the dopant ion concentration resulted in higher maximum sensitivities and narrowing the useful range of excitation power density. Similarly to Ln^{3+} doped materials, Cr^{3+} guarantees high photostability and sensitive luminescence-based quantification of temperature. Nevertheless, the most important advantages of Cr^{3+} ions over Ln^{3+} ions is their much higher absorption cross-section which is not compromised by the increasing temperature and more efficient self-heating. Moreover the larger spectral bandwidth of the absorption bands of Cr^{3+} enables a much wider spectral range of operation of such designed luminescence sensors. It should be noted here that the excitation density range of the Cr^{3+} based power meter depends on the energy separation between the ^2E and the $^4T_2$ states. Therefore, it can be optimized according to the requirements of specific applications by the intentional optimization of the crystal field strength affecting the Cr^{3+} ions through host material composition.

Conflicts of interest

There are no conflicts to declare.

Acknowledgements

This work was supported by the National Science Center Poland (NCN) under project No. 2019/35/N/ST5/00553. K. E.-P. acknowledges the START Fellowship from the Foundation for Polish Science. The authors acknowledge MSc. Zuzanna Korczak for help in carrying out the experiments.

References

1 E. G. Moore, A. P. S. Samuel and K. N. Raymond, From antenna to assay: Lessons Learned in Lanthanide Luminescence, *Acc. Chem. Res.*, 2009, **42**(4), 542–552, DOI: **10.1021/ar800211j**.
2 J. Li, J. Yan, D. Wen, W. U. Khan, J. Shi, M. Wu, Q. Su and P. A. Tanner, Advanced Red Phosphors for White Light-Emitting Diodes, *J. Mater. Chem. C*, 2016, **4**(37), 8611–8623, DOI: **10.1039/c6tc02695h**.
3 J. W. Stouwdam, G. A. Hebbink, J. Huskens and F. C. J. M. Van Veggel, Lanthanide-Doped Nanoparticles with Excellent Luminescent Properties in Organic Media, *Chem. Mater.*, 2003, **15**(24), 4604–4616, DOI: **10.1021/cm034495d**.
4 P. Netzsch, M. Hämmer, E. Turgunbajew, T. P. van Swieten, A. Meijerink, H. A. Höppe and M. Suta, Beyond the Energy Gap Law: The Influence of Selection Rules and Host Compound Effects on Nonradiative Transition Rates in Boltzmann

Thermometers, *Adv. Opt. Mater.*, 2022, **10**(11), 2200059, DOI: 10.1002/adom.202200059.

5 F. Kang, G. Sun, P. Boutinaud, H. Wu, F.-X. Ma, J. Lu, J. Gan, H. Bian, F. Gao and S. Xiao, Recent Advances and Prospects of Persistent Luminescent Materials as Inner Secondary Self-Luminous Light Source for Photocatalytic Applications, *Chem. Eng. J.*, 2021, **403**, 126099, DOI: 10.1016/j.cej.2020.126099.

6 W. Shao, G. Chen, T. Y. Ohulchanskyy, A. Kuzmin, J. Damasco, H. Qiu, C. Yang, H. Ågren and P. N. Prasad, Lanthanide-Doped Fluoride Core/Multishell Nanoparticles for Broadband Upconversion of Infrared Light, *Adv. Opt. Mater.*, 2015, **3**(4), 575–582, DOI: 10.1002/adom.201400404.

7 E. Song, Z. Chen, M. Wu, S. Ding, S. Ye, S. Zhou and Q. Zhang, Room-Temperature Wavelength-Tunable Single-Band Upconversion Luminescence from Yb3+/Mn2+ Codoped Fluoride Perovskites ABF3, *Adv. Opt. Mater.*, 2016, **4**(5), 798–806, DOI: 10.1002/adom.201500732.

8 M. G. Brik and C.-G. Ma, *Theoretical Spectroscopy of Transition Metal and Rare Earth Ions*, 2019, DOI: 10.1201/9780429278754.

9 A. Hauser and C. Reber Spectroscopy and Chemical Bonding in Transition Metal Complexes, in *Structure and Bonding*, ed. D. M. P. Mingos, Springer International Publishing, Cham, 2016, vol. 172, pp. 291–312, DOI: 10.1007/430_2015_195.

10 G. Fuxi and L. Huimin, Spectroscopy of Transition Metal Ions in Inorganic Glasses, *J. Non Cryst. Solids*, 1986, **80**(1–3), 20–33, DOI: 10.1016/0022-3093(86)90376-5.

11 J. Zhou, Z. Liu and F. Li, Upconversion Nanophosphors for Small-Animal Imaging, *Chem. Soc. Rev.*, 2012, **41**(3), 1323–1349, DOI: 10.1039/c1cs15187h.

12 J. Rocha, L. D. Carlos, F. A. A. Paz and D. Ananias, Luminescent Multifunctional Lanthanides-Based Metal–Organic Frameworks, *Chem. Soc. Rev.*, 2011, **40**(2), 926–940, DOI: 10.1039/c0cs00130a.

13 D. Yang, P. Ma, Z. Hou, Z. Cheng, C. Li and J. Lin, Current Advances in Lanthanide Ion (Ln^{3+})-Based Upconversion Nanomaterials for Drug Delivery, *Chem. Soc. Rev.*, 2015, **44**(6), 1416–1448, DOI: 10.1039/c4cs00155a.

14 Q. Xiao, X. Zheng, W. Bu, W. Ge, S. Zhang, F. Chen, H. Xing, Q. Ren, W. Fan, K. Zhao, Y. Hua and J. Shi, A Core/Satellite Multifunctional Nanotheranostic for in Vivo Imaging and Tumor Eradication by Radiation/Photothermal Synergistic Therapy, *J. Am. Chem. Soc.*, 2013, **135**(35), 13041–13048, DOI: 10.1021/ja404985w.

15 Y. Dai, H. Xiao, J. Liu, Q. Yuan, P. Ma, D. Yang, C. Li, Z. Cheng, Z. Hou, P. Yang and J. Lin, In Vivo Multimodality Imaging and Cancer Therapy by Near-Infrared Light-Triggered Trans -Platinum pro-Drug-Conjugated Upconverison Nanoparticles, *J. Am. Chem. Soc.*, 2013, **135**(50), 18920–18929, DOI: 10.1021/ja410028q.

16 H. Xing, W. Bu, S. Zhang, X. Zheng, M. Li, F. Chen, Q. He, L. Zhou, W. Peng, Y. Hua and J. Shi, Multifunctional Nanoprobes for Upconversion Fluorescence, MR and CT Trimodal Imaging, *Biomaterials*, 2012, **33**(4), 1079–1089, DOI: 10.1016/j.biomaterials.2011.10.039.

17 L. Marciniak, A. Pilch, S. Arabasz, D. Jin and A. Bednarkiewicz, Heterogeneously Nd^{3+} Doped Single Nanoparticles for NIR-Induced Heat Conversion, Luminescence, and Thermometry, *Nanoscale*, 2017, **9**(24), 8288–8297, DOI: 10.1039/c7nr02630g.

18 A. Skripka, V. Karabanovas, G. Jarockyte, R. Marin, V. Tam, M. Cerruti, R. Rotomskis and F. Vetrone, Decoupling Theranostics with Rare Earth Doped Nanoparticles, *Adv. Funct. Mater.*, 2019, **29**(12), 1807105, DOI: 10.1002/adfm.201807105.

19 A. Suchocki and R. C. Powell, Laser-Induced Grating Spectroscopy of Cr^{3+}-Doped $Gd_3Ga_5O_{12}$ and $Gd_3Sc_2Ga_3O_{12}$ Crystals, *Chem. Phys.*, 1988, **128**(1), 59–71, DOI: 10.1016/0301-0104(88)85062-6.

20 Z. Pan, Y. Y. Lu and F. Liu, Sunlight-Activated Long-Persistent Luminescence in the near-Infrared from Cr^{3+}-Doped Zinc Gallogermanates, *Nat. Mater.*, 2012, **11**(1), 58–63, DOI: 10.1038/nmat3173.

21 M. Grinberg, P. I. MacFarlane, B. Henderson and K. Holliday, Inhomogeneous Broadening of Optical Transitions Dominated by Low-Symmetry Crystal-Field Components in Cr3+-Doped Gallogermanates, *Phys. Rev. B*, 1995, **52**(6), 3917–3929, DOI: 10.1103/PhysRevB.52.3917.

22 W. Nie, Y. Li, J. Zuo, Y. Kong, W. Zou, G. Chen, J. Peng, F. Du, L. Han and X. Ye, Cr^{3+}-Activated $Na_3X_2Li_3F_{12}$ (X = Al, Ga, or In) Garnet Phosphors with Broadband NIR Emission and High Luminescence Efficiency for Potential Biomedical Application, *J. Mater. Chem. C*, 2021, **9**(42), 15230–15241, DOI: 10.1039/D1TC03763C.

23 W. Nie, L. Yao, G. Chen, S. Wu, Z. Liao, L. Han and X. Ye, A Novel Cr^{3+}-Doped $Lu_2CaMg_2Si_3O_{12}$ Garnet Phosphor with Broadband Emission for near-Infrared Applications, *Dalton Trans.*, 2021, **50**(24), 8446–8456, DOI: 10.1039/D1DT01195B.

24 D. Wu, L. Liu, H. Liang, H. Duan, W. Nie, J. Wang, J. Peng and X. Ye, $LiBAlF_6$:Cr^{3+} (B = Ca, Sr) Fluoride Phosphors with Ultra-Broad near-Infrared Emission for NIR Pc-LEDs, *Ceram. Int.*, 2022, **48**(1), 387–396, DOI: 10.1016/j.ceramint.2021.09.114.

25 M. Açıkgöz, C. Rudowicz and P. Gnutek, Temperature Dependence of Local Structural Changes around Transition Metal Centers Cr^{3+} and Mn^{2+} in $RAl_3(BO_3)_4$ Crystals Studied by EMR, *Opt. Mater.*, 2017, **73**, 124–131, DOI: 10.1016/j.optmat.2017.07.052.

26 G. Wang, T. P. J. Han, H. G. Gallagher and B. Henderson, Novel Laser Gain Media Based on Cr^{3+}-doped Mixed Borates $RX_3(BO_3)_4$, *Appl. Phys. Lett.*, 1995, **67**(26), 3906–3908, DOI: 10.1063/1.115313.

27 A. Szysiak, L. Lipińska, W. Ryba-Romanowski, P. Solarz, R. Diduszko and A. Pajaczkowska, Nanopowders of $YAl_3(BO_3)_4$ Doped by Nd, Yb and Cr Obtained by Sol-Gel Method: Synthesis, Structure and Luminescence Properties, *Mater. Res. Bull.*, 2009, **44**(12), 2228–2232, DOI: 10.1016/j.materresbull.2009.08.004.

28 M. Cheng, X.-X. Wu and W.-C. Zheng, Investigations of the Thermal Red-Shift of R_1-Line and the Electron-Phonon Coupling Parameter for Cr^{3+}-Doped $YAl_3(BO_3)_4$ Crystal, *Optik (Stuttg)*, 2017, **144**, 413–415, DOI: 10.1016/j.ijleo.2017.06.120.

29 Z. Ji-Ping, C. Gang and Z. Hua-Bin, Theoretical Studies of Energy Spectra and g Factors of Cr^{3+} -Doped $YAl_3(BO_3)_4$, *Commun. Theor. Phys.*, 2006, **45**(6), 1121–1125, DOI: 10.1088/0253-6102/45/6/031.

30 G. Wang, H. G. Gallagher, T. P. J. Han and B. Henderson, The Growth and Optical Assessment of Cr^{3+}-Doped $RX(BO_3)_4$ Crystals with R = Y, Gd; X = Al, Sc, *J. Cryst. Growth*, 1996, **163**(3), 272–278, DOI: 10.1016/0022-0248(95)00969-8.

31 M. G. Brik, V. A. Lebedev and E. V. Stroganova, Spectroscopic and Crystal Field Studies of (Ce,Gd)Sc3(BO3)4:Cr3+ Crystals, *J. Phys. Chem. Solids*, 2007, **68**(9), 1796–1804, DOI: 10.1016/j.jpcs.2007.05.002.

32 X. Long, Z. Lin, Z. Hu, G. Wang and T. P. J. Han, Optical Study of Cr^{3+}-Doped $LaSc_3(BO_3)_4$ Crystal, *J. Alloys Compd.*, 2002, **347**(1), 52–55, DOI: 10.1016/S0925-8388(02)00785-5.

33 X. Long, G. Wang and T. P. J. Han, Growth and Spectroscopic Properties of Cr^{3+}-Doped $LaSc_3(BO_3)_4$, *J. Cryst. Growth*, 2003, **249**(1), 191–194, DOI: 10.1016/S0022-0248(02)02073-0.

34 X. Long, Z. Lin, Z. Hu and G. Wang, Polarized Spectral Characteristics and Energy Levels of Cr^{3+}:$LaSc_3(BO_3)_4$ Crystal, *Chem. Phys. Lett.*, 2004, **392**(1), 192–195, DOI: 10.1016/j.cplett.2004.05.067.

35 H. Wu, L. Jiang, K. Li, C. Li and H. Zhang, Design of Broadband Near-Infrared Y0.57La0.72Sc2.71(BO3)4:Cr3+ Phosphors Based on One-Site Occupation and Their Application in NIR Light-Emitting Diodes, *J. Mater. Chem. C*, 2021, **9**(35), 11761–11771, DOI: 10.1039/D1TC01508G.

36 Q. Zhang, H. Ni, L. Wang and F. Xiao, Luminescence Properties and Energy Transfer of $GdAl_3(BO_3)_4$:Ce^{3+}, Tb^{3+} Phosphor, *Ceram. Int.*, 2016, **42**(5), 6115–6120, DOI: 10.1016/j.ceramint.2015.12.170.

37 Y. Yue, Y. Zhu, Y. Zhao, H. Tu and Z. Hu, Growth and Nonlinear Optical Properties of $GdAl_3(BO_3)_4$ in a Flux without Molybdate, *Cryst. Growth Des.*, 2016, **16**(1), 347–350, DOI: 10.1021/acs.cgd.5b01304.

38 J. He, S. Zhang, J. Zhou, J. Zhong, H. Liang, S. Sun, Y. Huang and Y. Tao, Luminescence Properties of an Orange-Red Phosphor $GdAl_3(BO_3)_4$:Sm^{3+} under VUV Excitation and Energy Transfer from Gd^{3+} to Sm^{3+}, *Opt. Mater.*, 2015, **39**, 81–85, DOI: 10.1016/j.optmat.2014.11.002.

39 L. J. Q. Maia, C. R. Ferrari, V. R. Mastelaro, A. C. Hernandes and A. Ibanez, Synthesis Optimization, Structural Evolution and Optical Properties of Y0.9Er0.1Al3(BO3)4 Nanopowders Obtained by Soft Chemistry Methods, *Solid State Sci.*, 2008, **10**(12), 1835–1845, DOI: 10.1016/j.solidstatesciences.2008.03.031.

40 C. R. Ferrari, M. Baccia, A. Ibanez and A. C. Hernandes, Thermal and Structural Investigation of Er:$YAl_3(BO_3)_4$ Nanocrystalline Powders, *J. Therm. Anal. Calorim.*, 2009, **95**(1), 59–62, DOI: 10.1007/s10973-007-8821-1.

41 B. Malysa, A. Meijerink and T. Jüstel, Temperature Dependent Luminescence Cr^{3+}-Doped $GdAl_3(BO_3)_4$ and $YAl_3(BO_3)_4$, *J. Lumin.*, 2016, **171**, 246–253, DOI: 10.1016/j.jlumin.2015.10.042.

42 K. Elzbieciak and L. Marciniak, The Impact of Cr^{3+} Doping on Temperature Sensitivity Modulation in Cr^{3+} Doped and Cr^{3+}, Nd^{3+} Co-Doped $Y_3Al_5O_{12}$, $Y_3Al_2Ga_3O_{12}$, and $Y_3Ga_5O_{12}$ Nanothermometers, *Front. Chem.*, 2018, **6**, 424, DOI: 10.3389/fchem.2018.00424.